UNIVERSITY OF TWENTE.

Faculty of Electrical Engineering, Mathematics & Computer Science

Analysis of Radio Propagation Inside the Human Body for in-Body Localization Purposes

Ilka Dove

M.Sc. Thesis
August 2014

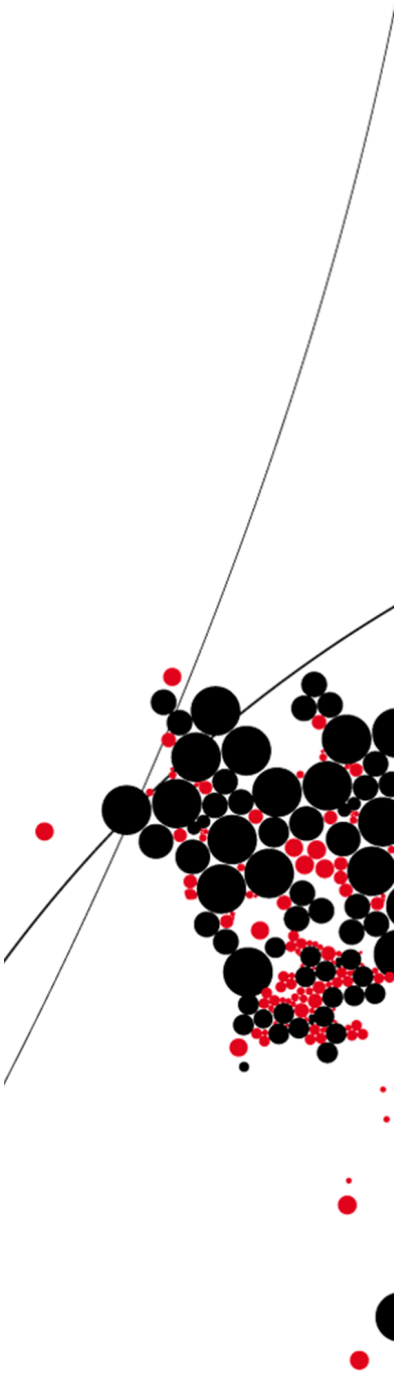

Supervisors:
dr. ir. M. J. Bentum
prof. dr. ir. F. B. J. Leferink
dr. ir. A. Meijerink
prof. dr. ir. R. J. A. van Wezel

Telecommunication Engineering Group
Faculty of Electrical Engineering,
Mathematics and Computer Science
University of Twente
P.O. Box 217
7500 AE Enschede
The Netherlands

Analysis of Radio Propagation Inside the Human Body for in-Body Localization Purposes

I. Dove B.Eng., Telecommunication Engineering Group,
Faculty of Electrical Engineering, Mathematics and Computer Science, University of Twente

***Abstract*—Health care is getting a lot of attention. Especially due to population aging, health care has to be made affordable in the future. There is a need for enabling in-body communication and also localization of sensors which are moving through the human body. The propagation of radio frequency signals through different layers of human tissue is analyzed. In contrast to other research the complex characteristics of human tissue are included for both received signal strength and time of arrival methods. A multilayer model is developed to investigate the influences of different tissue layers on the absolute signal attenuation and travel time for signal propagation from in-body to on-body for in-body communication allocated frequencies: 403.5 MHz, 916.5 MHz, and 2.45 GHz. The analysis results show that the attenuation and delay in small intestine and muscle tissues have more influence on the total values than in fat tissue.**

***Index Terms*—In-body propagation, multilayer model, RF tissue characteristics, lossy medium**

I. Introduction

World wide, every day about 160 thousand sixtieth birthdays are celebrated. This is equivalent to 58 million sixtieth birthdays in a year and the number is even growing. In 2012, 810 million people, or 11.5 percent, of the global population were older than 59 years. This percentage is expected to grow to 2 billion (and therefore 22 percent of the population) in 2050. Today the only country with more than 30 percent elderly people (>60 years) is Japan. By 2050, 64 additional countries will reach this percentage [1]. Due to aging of the world population more and more people will not be able to go to the doctor's practice anymore. A solution is on distance provided health care in the future. The aging of the population creates the need for new health care structures, and simpler and faster surgery.

Today an increasing number of health care products are developed to make life easier for patients and doctors. An example of this is capsule endoscopy which can replace normal endoscopy whereby the intestinal tract is reviewed to search for disorders. Normal endoscopy causes discomfort for the patients, and not even the whole tract can be reviewed [2]. By means of technologies such as IC Technology, small cameras, and LED techniques, endoscopy pills can be made small enough to be swallowed [2]. Due to this the analysis of diseases in the human tract is made easier. The whole human tract can be analyzed by capsule endoscopy, which has advantages such as lower risks and lower hospitalization and resection rates for the patients [3]. The capsule endoscopy is also of great importance for the detection of obscure bleeding, among other diseases, which cannot be observed in the bowel movement and occurs in the small intestine (SI) [4].

Devices such as the endoscopy capsule which transmit data can be considered as part of a body area network (BAN). BAN is a network concept to set up connections around a human who carries communication devices. This network can consist of a number of devices or sensors which communicate with each other. One can distinguish three forms of BANs: off-body, on-body, and in-body communications [5], [6]. Figure 1 shows an overview of the different possible communication constellations and the communication areas of BANs. The communication between a sensor and a device near the body is called off-body communication. On-body communication is the communication between devices which are located on the body. The communication usually takes place wirelessly around the body, via the environment (which is the most prominent communication channel) or via creeping waves on the body surface. In-body communication is the communication from a sensor or device which is located inside the body to another device in the body or on the surface of the body.

Localization of sensors is desired to make a proper interpretation of the measured values possible. Knowing the location of the capsule and the detected values leads to much better treatments of diseases. Parts of the human body, such as the complete SI of the tract, could not be reached before using traditional endoscopy. Spinning and backwards movements of the capsule and the filling and emptying cycle of the human tract make it difficult to determine the position of the pill from the taken images [7]–[9]. Therefore, there is a need for an alternative localization method.

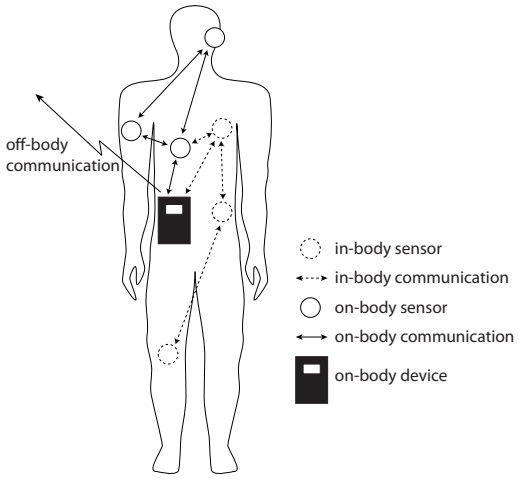

Fig. 1: An overview of a BAN communication

An example of an existing and commonly used localization system for positioning in free space is the Global Positioning System (GPS). Other systems which are available use radars to determine the ranges of objects to the system. These techniques are well developed and are reliable. A localization technique for locating persons or devices in a room is already more challenging due to the multipath environment. The environment is varying and reflections make it difficult to extract the transmitted signal from the received signals. In-body sensor localization is even more challenging, due to the human body which acts as a challenging propagation medium. The human body consists of many different types of tissue each having their own propagation characteristics. Knowledge of localization techniques and signal propagation in media have to be combined to develop an in-body localization method.

To gain more insight into the in-body signal propagation this thesis studies radio frequency (RF) propagation inside the human body.

This physical insight has to be obtained to estimate the channel properties which are required for later localization steps. The behavior of RF propagation for different frequency dependent tissue layers for multiple frequencies is analyzed. A layered model is developed by means of which the travel times and attenuations of the propagating signals are studied. In contrast to other research, no simulations or measurements with a "complete" communication system are performed. The results of those simulations or measurements do not give information on the travel time and attenuation which are caused only by the material characteristics. Therefore there is a demand for an analysis of the in-body to on-body propagation medium to make a step towards affordable and reliable in-body applications.

The structure of this thesis is as follows. This section is followed by the introduction to the theoretical background, Section II, which provides an overview of the important topics for in-body communication, propagation and localization. A physical channel model is presented in Section III which is followed by an analysis in Section IV. Conclusions and recommendations of the physical multilayer model for in-body localization purposes are formulated in Section V.

II. Background

Technical background information about important restrictions and challenges for in-body communication is provided in Section II-A. Possible solutions and methods for the localization of sensors are given in Section II-B, and existing propagation models which describe the in-body communication channel are presented in Section II-C.

A. In-body communication

The restrictions regarding an in-body communication system which have to be considered when setting up a BAN are introduced in this section to obtain a better understanding of the complexity for communication inside the human body.

In-body communication requires a specific communication system. A communication system includes transmit and receive devices which work at a suitable frequency for the communication environment. The antennas for example must be designed considering the environment. Additionally, the propagation medium has to be known to enable viable communication.

The human body is a complex system consisting of many different kinds of tissues. These tissues are constructed in a layered way where the thickness is different for each tissue and differ for each human. Capsule endoscopy (or other analyzing sensors) communicate from inside the body to the outside of the body. Therefore, the tissues which are present in the human torso have to be taken into account for these applications. An example of a cross sectional image produced by means of a magnetic resonance imaging (MRI) scan of a human torso can be seen in Figure 2. The description of the many different tissue types and combinations is challenging. An additional challenge for a good estimation of the channel is the high dissipation of RF signals due to the characteristics of the body tissues. Along with these characteristics comes the fact that the propagation speed varies over the different tissue layers. The channel can be estimated by propagation models suggested in literature (Section II-C) or by analysis of the physical channel medium as it is proposed in this research. As a result of the different tissue layers multipath reflections occur. Moreover, the layers are continuously changing due to the continuous movements of the whole body and the gastrointestinal tract. The analysis of the RF propagation channel inside the human body is therefore challenging [11], [12]. To determine the channel parameters, the different tissue characteristics have to be specified. In [13] the dielectric properties, relative permittivity and conductivity, of 57 different tissues were analyzed for RF and microwave frequencies (10 Hz – 20 GHz). The authors of [14] present a calculation of the tissue properties based on [15].

Another point which has to be considered is the choice of operation frequency. The electrical properties of the human tissue, the application type, the required transmission bandwidth, the available space for the antenna, and the allocated bands are of importance for the frequency choice. There are restrictions made by different instances for different countries. The frequency band of 402–405 MHz is allocated for im-

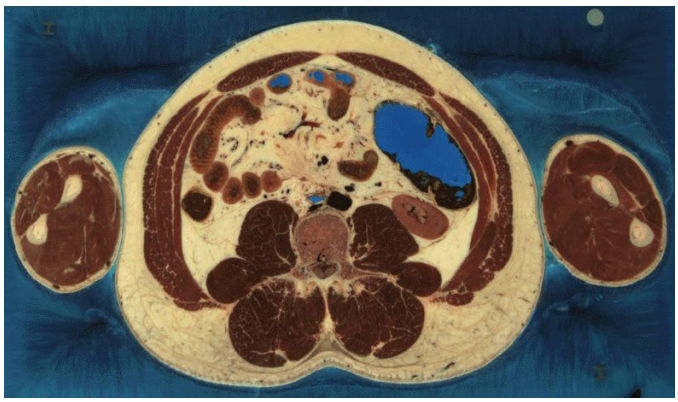

Fig. 2: Cross section of a human male torso [10]

plantable medical devices and is called the Medical Implant Communication Service (MICS) band. The MICS band is defined by the U.S. Federal Communications Commission (FCC) and the European Telecommunications Standards Institute (ETSI) [16]. In 2009 the FCC defined the Medical Radio (MedRadio) band which is in the range of 401–406 MHz for Europe and is centered around 916.5 MHz for the U.S.. An additional allowed band for BANs or medical applications is the industrial, scientific and medical (ISM) 2.45 GHz radio band which is used in the IEEE 802.15.6 standard [17]. In [18] an overview of the different communication scenarios and frequencies of the standard is presented. In literature research on ultra-wideband (UWB) communications between 3.1 and 10 GHz for in-body applications is described as well [19]–[21]. However, UWB is not standardized in the frequency allocation for medical applications. The power level of UWB communications is actually below the noise floor which means that it is harmless to humans. Consequently, the receivers must be able to receive these very low power levels. Furthermore, there is a great variance of permittivity and conductivity over the large bandwidth of UWB which has to be taken care of for the description of the channel [18]. Therefore, no UWB signals are considered in this thesis.

Besides the decision for a frequency, an antenna which works inside the body has to be chosen or developed. The antenna is an important part of the communication system, since in-body communication is always performed wireless for applications as the capsule endoscopy. Wires are not desirable, or even possible to connect a device from inside the body to a device on the outside. In some cases the device inside the body should also be powered via the same wireless link. In standard RF applications the antenna design depends mostly on the frequency but regarding the in-body application the antenna is limited in size and the RF transmission challenges inside the human body [22]. The communication channel inside the human body is completely different from that in free space, because of the material properties. The wavelength inside human body tissue is different from the wavelength in free space. Therefore the size of the antenna is different for in-body applications. Furthermore, the directivity of the antenna is a challenging part because the properties of the human body tissues have impact on the antenna radiation pattern. Another design limitation which comes along with placing antennas inside the human body is that the antenna must be of non-corrosive and bio-compatible material (e.g. platinum or titanium [6]). Electric field components of the transmitted RF waves produce heating of the body tissue. The limitations for heating body tissue are described by the maximum Specific Absorption Rate (SAR) which specifies an amount of absorbed power per gram of body weight. The value of this rate is restricted by different instances for different parts of the human body. The SAR limitations are given by the regulations of the FCC and the International Commission on Non-Ionizing Radiation Protection (ICNIRP) (see Table I).

Setting up a BAN is challenging. Mismatches of antennas and influences of the communication devices on the channel propagation cannot simply be avoided and will therefore be present. These influences cannot be extracted from simulations and measurements. With this information on in-body communication kept in mind the analysis of a physical channel model will lead to absolute attenuations and transmit times of an RF signal independent of the implemented BAN.

B. Localization

Modern localization for capsule endoscopy is based on image recognition. Programs analyze images taken by the capsule based on colors, textures and shapes of the tract images [24]–[26]. The images have to be reviewed by the doctor to determine the position of the diseases or abnormalities in the human tract. This analysis is time consuming [25]. Therefore an alternative for localization is needed and for this RF ranging is considered.

Localization actually consists of two steps. The first step is to measure and interpret the signal. This is called ranging. After collecting measurement data from multiple radio links, geometric methods can be used to calculate the position of the target. This second step is referred to as fusion. Techniques based on the range estimation by time of arrival (TOA) or received signal strength (RSS) and angle of direction measure with angle of arrival (AOA) are most common. Alternative techniques like applying fingerprinting are used to improve the location estimation.

The traveled distance can be calculated from the time and the propagation speed in the medium or from signal strengths and the channel characteristics. To determine the position from the ranging data most of the localization techniques make use of methods like trilateration, triangulation and multilateration. However, these methods are nontrivial and require a good knowledge of the communication medium.

Range estimation with TOA measurements makes use of the time difference which occurs between transmitting and receiving the signal. Precise synchronization between the devices is needed for this technique. When no synchronization is available two-way TOA measurements can be used to calculate the travel time between the two devices, but for this an accurate clock time is required as well. RSS measurements make use of the signal strength which is measured at the receiver. The transmitted and received signal strength are known and in combination with a known environment, the attenuation can be linked to the traveled distance. An estimation of the medium characteristics can be made from attenuation measurements and the distance. Measuring the AOA is a technique to determine the direction from which a signal is coming. A good knowledge of the propagation medium is desired for this technique as well. Additionally, accurate measurement devices are required and all measurement equipment must be synchronized. The AOA technique is generally not suitable for in-body communications. It is not even used for indoor localization because it suffers much from the continuously changing fading and multipath of the environment [8], [9].

Challenges of TOA measurements regarding the body properties and the channel are analyzed in [12]. A comparison of TOA and RSS-based localization techniques is presented in [27] by making a finite-difference time-domain (FDTD) simulation with MATLAB and a finite element method (FEM)

TABLE I: SAR regulations [23]

	SAR in W/kg (Whole Body Average)	SAR in W/kg (Head/Trunk)	SAR W/kg (Limbs)	Induced E in V/m (All Tissue)	Induced J in mA/m^2 (Central Nervous System)
FCC	0.08	1.6 (1 g)	4 (10 g)	–	–
ICNIRP2010	0.08	2.0 (10 g)	4 (10 g)	$1.35\ 10^{-4} f$ (f in Hz)	–
ICNIRP1998	0.08	2.0 (10 g)	4 (10 g)	–	$f/500$ (f in Hz)

simulation with HFSS. Unpredictable errors occur due to shadowed fading conditions and multipath propagation which is present inside the human body. These could be compensated by using a UWB technique which has a higher resolution for range estimation [28]. However, due to the wide frequency range and the frequency dependent characteristics of the medium an accurate range determination by UWB methods is challenging.
To make estimation more accurate tracking can be implemented. Additional comparison of the measured position with the previous position(s) to decide which points are possible would make the system robust against fading and environmental changes.

C. Propagation models

A channel model is required to enable calculations of the distance between transmitter and receiver possible. For in-body applications the travel time and signal attenuation are dependent on the different tissues through which the signal is propagating. To determine the position of a device inside the human body with localization methods described in the previous section, a channel model is required.
Several authors have published proposals of channel models for in-body communication. However, most of the models are based on simulation or measurement results for on-body purposes. The relevant models for this research are those that focus on implant to on-body communication.
The analysis of the channel inside the human body is difficult due to the different tissue types, boundaries between the tissue types, and variation of tissue thicknesses for each human [11], [12]. Simulations for field propagation inside the human body were performed by FDTD or FEM simulation tools. These tools give insight in the field distributions. A radio channel characterization and model for wireless implants for 402, 868 and 2400 MHz are presented in [29], together with the determination of the path loss exponent for in-body to on-body communications. The result of the research in [30] is the frequency dependency of the radiation pattern in posterior directions and field reduction due to the hips. In situ measurements show a power absorption of 19–25 dB and a rapid increase of the absorption for frequencies above 500 MHz [31]. The rapid increase is due to the salty characteristics of the tissues and consequently higher relative conductivity and permittivity of human tissue [32]. Following the results of the measurements in the human intestine, in-body communication has the least attenuation for frequencies between 450 and 900 MHz [33].
Based on the results of RSS measurements for the ISM and MICS bands a path loss model was developed from a capsule sized signal generator to a body worn antenna [34]. The measured RSS of the ISM band was on average 15 dB lower than the RSS of the MICS band. Other papers provide results from simulations and measurements of the fields of antennas around the human body and head [29], [30], [35]–[39].
In [19] UWB channel impulse responses of three different human models are investigated. For the channel models they refer to [11], where a path loss model of the IEEE 802.15.4a channel model and an impulse response description are used. A path loss model is developed in [34] from CT X-ray images, whereby a calculation of average relative permittivity of the human body together with the loss in air and reflection loss is extracted.
For a TOA based ranging technique the channel model makes use of the propagation speeds of the signals in the different tissue layers. For simulation and calculation purposes many papers calculate the average velocity of the propagating signal based on [40]–[43]:

$$v_{\text{avg}} = \frac{c}{\sqrt{\varepsilon_{\text{avg}}}}, \tag{1}$$

$$\varepsilon_{\text{avg}} = \sum_{i=1}^{N=1} r_i \varepsilon_i \text{ with } r_i = \frac{d_i}{d_{\text{total}}}, \tag{2}$$

with ε_i the relative permittivity of the ith layer. The authors of the papers [40], [43] rely on (2) to calculate the average relative permittivity of a layered structure of N tissues. Furthermore, a ratio r_i is given to the different tissues which accounts for the tissue thickness d_i of the ith layer with respect to the total travel path length d_{total}. In [40] MRI scans were applied to determine the tissue thicknesses before measuring the TOA values. In a second stage the TOA data from four nodes was used to calculate the position of an implant using a least squares (LS) method. In a later published paper the average velocity is calculated by [42]:

$$v_{\text{avg}} = \frac{c}{\sum_{i=1}^{N} r_i \sqrt{\varepsilon_i}}, \tag{3}$$

with the same variable definitions as in (2). The average tissue characteristics have to be determined before taking the square root and calculating the velocity of propagation. First summing up the relative permittivities and then calculating the propagation speed will not lead to the same results as first taking the square root of the material permittivities and summing up. The denominator of (3) describes the average propagation time. Once the propagation time is known the propagation velocity can be calculated. Therefore this way of averaging the propagation velocity is more rational.
A path loss model can be applied for an RSS based ranging

method. Such a model for medical implant communications was developed from simulation results by the National Institute of Standards and Technology (NIST) and proposed to the IEEE for the 802.15 MICS standard in September 2008 and published in [44]. The path loss $PL(d)$ at a certain distance d is defined by:

$$PL(d) = \frac{G_{\mathrm{R}} P_{\mathrm{T}}}{P_{\mathrm{R}}(d)}, \tag{4}$$

with the transmitted power P_{T}, the antenna gain of the receiver G_{R} and received power $P_{\mathrm{R}}(d)$. For the MICS band the antenna gain of the transmitter G_{T} is included in the channel part. The path loss $PL(d)$ in dB is modeled in a statistical way by:

$$PL_{\mathrm{dB}}(d) = L_{\mathrm{dB}}(d_0) + 10n \log \frac{d}{d_0} + S. \quad \text{for } d > d_0 \tag{5}$$

The path loss at a distance d is calculated from the loss at a reference distance $L_{\mathrm{dB}}(d_0)$, the path loss exponent n and a Gaussian random variable S with zero mean and standard deviation σ_s. S is included to correct for deviations due to bones and tissue materials as well as for antenna gain variations in different directions. The reference distance loss for $d_0 = 50$ mm is investigated for deep tissue and near surface applications. Furthermore, the path loss exponent and standard deviation values are found by implant to body surface modeling. The observed values for the path loss calculations of (5) are shown in Table II. The investigated deep tissue values are proposed for endoscopy applications and near surface results for implantable sensors for example pacemakers and motion sensors. For MICS channels the transmit antenna is considered as a part of the channel. The parameters S, $PL(d_0)$ and n of the model described by (5) are determined separately. The path loss parameters are determined within 20 mm of the skin. Simulations with 2 mm and 10 mm distance from the skin gave approximately the same values. The model is obtained by simulation which means that it is not verified by measurements or other physical experiments. [12], [45]–[47] refer to the same path loss model as the MICS standard. Others compare FDTD simulations with the path loss model of MICS which was gathered by FEM simulations [48]. It has to be pointed out that the MICS path loss model does not take the tissue properties into consideration [49].

Most of the localization and propagation models mentioned in this section make use of simulations. However, from simulations it cannot be concluded which parts of the communication system introduce the most significant path loss. Furthermore, it is unclear whether antenna matching is applied or not. From these simulations no general attenuation from the inside to the outside of the human body can be extracted. The propagation models for TOA ranging techniques make use of the tissue properties to calculate the propagation time, those for RSS do not. Thus, there is a lack of information on the influence of the human body characteristics on the attenuation of the signal to make an accurate ranging analysis.

In the following section a new physical channel model is introduced for RF TOA and RSS ranging which includes individual tissue properties.

TABLE II: Parameter values for the statistical path loss model of (5) for 403.5 MHz [44]

Implant to body surface	$L_{\mathrm{dB}}(d_0 = 50\ \mathrm{mm})$	n	σ_s[dB]
Deep tissue	47.14	4.26	7.85
Near tissue	49.81	4.22	6.81

III. Physical Channel Model

To estimate the range accurately, a model of the in-body propagation channel is required. Such a channel model enables an estimate of the range from measurement results. For a numerical analysis of the propagation channel a physical channel model is developed and introduced in this section.

To be able to describe the channel through which the signal has to propagate the medium should be known. The tissue constellation of the human torso can be figured out by analyzing images of humans from for example CT or MRI scanners. However, using such an image analysis for the localization of an endoscopy capsule, would insert an additional step to the localization mechanism which costs time, needs appropriate equipment and requires trained personnel. Therefore, a model of the average tissue constellation of the human body should be made to spare time and costs. Because of the many different layers and layer constellations of tissues of the human torso, as shown in Figure 2, a simplification of the structure has to be made. A basic layered model can be created which contains the usually present main tissues of the human torso. In first instance a one dimensional layer model together with a distinction of different groups of human types can be considered. The advantage of such a method is that a CT or MRI scan is unnecessary before the system can be used. This is essential for a simple usage of capsule endoscopy.

For this research a multilayer model with N layers is made to resemble the tissue constellation of a human torso. Making use of such a layered model, the number of tissue layers can be easily extended depending on the purpose of the model. The basic tissue layers of a human body from the inside to the outside are: SI, visceral fat (fat 1), abdomen muscle, subcutaneous fat (fat 2) and skin. Therefore, this multilayer model has $N = 5$ layers. It is shown in Figure 3. The different tissue layers have the following numbers: SI $i = 1$, fat 1 $i = 2$, muscle $i = 3$, fat 2 $i = 4$, skin $i = 5$. Air is assumed on the outside and is therefore the sixth layer. Those different tissue layers have different thicknesses which are varying from a millimeter to several centimeters. Table III gives an overview of three different human types which are defined based on

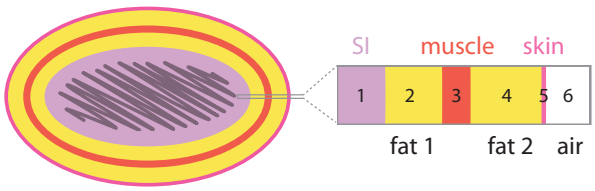

Fig. 3: Multi layer simplification cross section of human torso and multilayer model

the amount of visceral fat. Type 1 with the lowest amount, Type 2 with medium amount, and Type 3 with highest amount of visceral fat [9]. The location of the endoscopy capsule is assumed to be in an outer twist of the SI, and thus not in the scribbled part of the SI as shown in Figure 3. Therefore, the thickness of the SI layer is for this research fixed to 10 mm. The location of the on-body device is assumed to be directly placed on the skin which means that the thickness of the air layer is equal to 0 mm.
This layer model will be used to estimate the absolute attenuation, and propagation times of RF signals propagating from an in-body device to an on-body device. The next section describes the propagation of waves for different material characteristics. The advantages of such a one dimensional multilayer model is that the analysis of the signal propagation can start with a basic numerical model which can be easily extended to a more advanced analysis. In many cases in literature, simulations are performed which provide results on the total propagation times and attenuations of the signal. These simulations do not provide information on the influences of the different tissue layers with their complex characteristics. To make a numerical analysis of the multilayer model, the propagation of a wave inside the human body should be known. The next section therefore provides an analysis and derivation of the wave propagation properties as well. For this analysis it is assumed that the layers are infinitely wide, the interfaces are parallel to each other, the media are isotropic and homogeneous, and the propagation of the signal is normal to the interfaces.

IV. Analysis

The radio propagation inside the introduced physical channel model is investigated in this section. This section is divided into three parts. First a general analysis of waves propagating in lossy materials in IV-A. In IV-B and IV-C the analysis of the multilayer model for TOA and RSS is performed. For the RSS analysis only the attenuations which occur due to the propagation model are calculated, not a path loss as is done in literature.

A. Waves in lossy material

The propagation behavior of an RF wave depends on the permeability, permittivity, and conductivity characteristics of the medium.

TABLE III: Tissue thickness variation for different human dimensions [9]

Tissue	Range of thickness (mm)		
	Type 1	Type 2	Type 3
Small Intestine	10	10	10
Visceral fat (Fat 1)	$15-36$	$37-47$	$47-98$
Abdomen muscle	$8-16$	$8-16$	$8-16$
Subcutaneous fat (Fat 2)	$17-34$	$17-34$	$20-33$
Skin	$1.1-1.6$	$1.1-1.6$	$1.1-1.6$
Air	0	0	0
Total	$51.1-97.6$	$73.1-108.6$	$86.1-158.6$

The ideal case, as it is considered in most literature, is the propagation in lossless materials. Tissues of the human body however are lossy materials due to their characteristics. Lossy materials do not only have a real part of the permittivity but also an imaginary part which contributes to the calculations of the propagation speed, attenuation, reflections, and transmission parameters. However, most literature on in-body communication does not take these complex characteristics into account. The analysis in this thesis also includes the imaginary part of the parameters such that a good estimation of the attenuations and reflections of the different tissues can be made in the following sections. In literature it is often unclear whether to apply only the real part of the permittivity or the imaginary part to calculate the propagation constant of the propagating waves in a material as well. Therefore, the definitions and derivations for the calculations of the complex propagation constant are deduced from general expressions and clearly explained in this section.
A plane electromagnetic wave traveling in a positive one dimensional direction can be described by:

$$E(z) = Ee^{-\gamma z}, \tag{6}$$

where E is the complex amplitude of the signal at $z = 0$, z the propagation distance and γ the complex propagation constant. In general the complex propagation constant γ of a wave can be specified as [50], [51]:

$$\gamma = j\omega\sqrt{\mu\varepsilon}, \tag{7}$$

with $\mu = \mu_{\mathrm{r}}\mu_0$ the permeability of the material, which is equal to μ_0 because $\mu_{\mathrm{r}} = 1$ for biological materials, and the permittivity $\varepsilon = \varepsilon_0\varepsilon_{\mathrm{r}}$.
The relative permittivity ε_{r} of human body tissue is complex because the conductivity σ is not zero. The relative permittivity is not only complex but also frequency dependent. The relative permittivity has to be described by:

$$\varepsilon_{\mathrm{r}}(\omega) = \varepsilon'_{\mathrm{r}}(\omega) - j\varepsilon''_{\mathrm{r}}(\omega), \tag{8}$$

with $\varepsilon'_{\mathrm{r}}$ the real part and $\varepsilon''_{\mathrm{r}}$ as the imaginary part of the relative permittivity. From this the permittivity can be expressed as:

$$\varepsilon(\omega) = \varepsilon'(\omega) - j\varepsilon''(\omega) = \varepsilon'_{\mathrm{r}}(\omega)\varepsilon_0 - j\varepsilon''_{\mathrm{r}}(\omega)\varepsilon_0. \tag{9}$$

Only the values of the real relative permittivity, conductivity, and sometimes the loss tangent of human tissue are provided in the literature. An overview of the real relative permittivity $\varepsilon'_{\mathrm{r}}$ (dimensionless) and the conductivity σ (siemens per meter) of some tissue types at the officially allocated frequencies is shown in Table IV. From the table it can be concluded that the tissue properties are frequency dependent as stated earlier. The imaginary part of the complex relative permittivity can be determined from the angular frequency ω and the conductivity σ by:

$$\varepsilon''_{\mathrm{r}}(w) = \frac{\sigma}{\omega\varepsilon_0}. \tag{10}$$

The imaginary part of the complex relative permittivity can also be calculated from the loss tangent and the real relative

TABLE IV: Electrical tissue parameters for selected tissues based on [15]

Tissue	403.5 MHz		916.5 MHz		2.45 GHz	
	σ	$\varepsilon'_{\mathrm{r}}$	$\sigma]$	$\varepsilon'_{\mathrm{r}}$	σ	$\varepsilon'_{\mathrm{r}}$
Skin	0.69	46.71	0.87	41.32	1.46	38.01
Fat	0.041	5.58	0.05	5.46	0.10	5.28
Muscle	0.8	57.1	0.95	54.99	1.74	52.73
SI	1.90	66.05	2.17	59.38	3.17	54.425
Colon	0.86	62.53	1.09	57.86	2.04	53.88
Nerve	0.45	35.37	0.58	32.48	1.09	30.15

permittivity of the material. The loss tangent is defined as the ratio of the imaginary permittivity and the real permittivity:

$$\tan\delta = \frac{\varepsilon''}{\varepsilon'} = \frac{\varepsilon''_{\mathrm{r}}}{\varepsilon'_{\mathrm{r}}}. \tag{11}$$

Consequently, the loss tangent is a measure for how lossy the material is. The higher the loss tangent the lossier the material is. The loss tangents of different human tissues are also given in [14].

According to (9) the complex relative permittivity of different tissue layers of the model are calculated and shown in Table V for the three frequency bands (403.5, 916.5 MHz and 2.45 GHz). In the calculations the properties of visceral fat (fat 1) are considered equal to those of the subcutaneous fat (fat 2). This will also be assumed in all further analyses.

By inserting (9) into (7) γ can expressed as:

$$\gamma = j\omega\sqrt{\mu\varepsilon'}\sqrt{1 - j\frac{\sigma}{\omega\varepsilon'}}. \tag{12}$$

The complex propagation constant can also be expressed as:

$$\gamma = \alpha + j\beta, \tag{13}$$

where the real part describes the attenuation constant α of the wave and the imaginary part the phase constant β. With (13) the impedance, skin depth, wavelength, and phase velocity can be determined. The attenuation and phase constant can be extracted from (12) and are obtained by:

$$\alpha = \omega\sqrt{\frac{\mu_0\varepsilon_0\varepsilon'_{\mathrm{r}}}{2}\left[\sqrt{1 + \left(\frac{\sigma}{\omega\varepsilon_0\varepsilon'_{\mathrm{r}}}\right)^2} - 1\right]}, \tag{14}$$

and

$$\beta = \omega\sqrt{\frac{\mu_0\varepsilon_0\varepsilon'_{\mathrm{r}}}{2}\left[\sqrt{1 + \left(\frac{\sigma}{\omega\varepsilon_0\varepsilon'_{\mathrm{r}}}\right)^2} + 1\right]}, \tag{15}$$

TABLE V: Complex relative permittivity

Tissue	403.5 MHz	916.5 MHz	2.45 GHz
SI	$66.05 - 84.68j$	$59.38 - 42.60j$	$54.43 - 23.27j$
Fat 1	$5.58 - 1.83j$	$5.46 - 1.01j$	$5.28 - 0.73j$
Muscle	$57.10 - 35.66j$	$54.99 - 18.65j$	$52.73 - 12.77j$
Fat 2	$5.58 - 1.83j$	$5.46 - 1.01j$	$5.28 - 0.73j$
Skin	$46.71 - 30.75j$	$41.32 - 17.08j$	$38.01 - 10.72j$

which is in agreement to the formulas in [50], [52]. These two formulas now clearly indicate how to make use of the complex permittivity and the conductivity to describe the effects on a plane wave when propagating in lossy material. The formulas assume there are no losses due to magnetic characteristics which is true for all human tissues as $\mu_{\mathrm{r}} = 1$.

The phase constant is a measure of the phase shift of the signal. The wavelength and the phase velocity can be determined from the phase constant as $\lambda = 2\pi/\beta$ and $v_{\mathrm{p}} = \omega/\beta$ respectively.

Now that the wave propagation properties for the propagation in lossy material are known, an analysis of the travel time and the attenuation of a signal from in-body to on-body can be performed. For these analyses, wave propagation normal to the developed one dimensional multilayer model is assumed as well as homogeneous materials and smooth layer boundaries. In the next section the travel time will be analyzed.

B. Travel time

For the TOA localization method the time it takes for the signal to propagate from inside the human body to outside the body should be estimated. From the propagation speed of the traveling wave together with the travel time the distance can be calculated.

The propagation speed of the waves inside the body are dependent on the permittivity and the conductivity of the medium as described in Section IV-A. In a lossless frequency independent medium, the propagation speed or phase velocity of a electromagnetic wave can be calculated by:

$$v_{\mathrm{p}} = \frac{1}{\sqrt{\mu\varepsilon}} = \frac{1}{\sqrt{\mu_0\varepsilon_0\mu_{\mathrm{r}}\varepsilon_{\mathrm{r}}}} = \frac{c_0}{\sqrt{\mu_{\mathrm{r}}\varepsilon_{\mathrm{r}}}}, \tag{16}$$

where $\mu_{\mathrm{r}} = 1$ and c_0 is the propagation speed in free space this corresponds to (1) as stated in Section II-C.

However, the propagation speed of an RF wave in lossy media is frequency dependent and not only depends on the permittivity but also on the conductivity. Hence, there is a group and a phase velocity which must be considered. These velocities should be calculated from the angular frequency ω and the phase constant (15). The phase velocity of an electromagnetic signal is defined as follows [50]–[52]:

$$v_{\mathrm{p}} = \frac{\omega}{\beta}. \tag{17}$$

The group velocity which is the actual propagation speed of the wave can be calculated by [51]:

$$v_{\mathrm{g}} = \frac{\partial\omega}{\partial\beta} = \left(\frac{\partial\beta}{\partial\omega}\right)^{-1}, \tag{18}$$

with the derivative of the phase constant β at an angular frequency ω. The propagation speed therefore depends on the permittivity, conductivity, and the angular frequency for both the phase and the group velocity. The group velocity of the different tissue materials for different frequencies are given in Table VI. The derivative of the group velocity is calculated by the difference quotient. From the results in the table it can be concluded that the in-body propagation speed is much lower than in free space (10^8 m/s). The group velocity values shown in the table vary from about 10% of the free space

TABLE VI: Phase velocity of different tissue layers and different centre frequencies

Tissue	Group velocity v_g in 10^8m/s		
	403.5 MHz	916.5 MHz	2.45 GHz
SI	0.3077	0.3815	0.4336
Fat 1	1.3783	1.3800	1.3817
Muscle	0.4005	0.4385	0.4488
Fat 2	1.3783	1.3800	1.3817
Skin	0.4383	0.4992	0.5288

propagation speed for 403.5 MHz in the SI tissue to 45% of c_0 for 2.45 GHz in fat tissue. The propagation speed in SI tissue varies 30% between the MICS frequency and the ISM frequency. For the fat tissue this variation is only 1%, the difference is 10% for muscle, and 17% for skin. From the small variations in propagation speed for different frequencies of fat and muscle tissue it can be concluded that there will be almost no differences in the propagation time of these layers when traveling through these layers for all frequency bands.
For the calculation of the total travel time of the wave from in-body to on-body, the time which is needed to propagate through each layer of the model (see Figure 3) has to be calculated and summed. To calculate the travel time of each layer the thickness of the regarding layer has to be divided by the propagation velocity of the regarding layer. The propagation time of the signal in each tissue layer can be calculated by:

$$t_i = \frac{d_i}{v_{g_i}}, \tag{19}$$

with the tissue thickness of the ith layer d_i in meters and the propagation speed v_g in meters per second. Therefore the total propagation time can be calculated by:

$$t_{\text{total}} = \sum_{i=1}^{N} \frac{d_i}{v_{g_i}} = \sum_{i=1}^{N} t_i. \tag{20}$$

The travel time for the different human types for the 403.5 MHz are shown in Table VII. From travel time of the different tissue layers and thicknesses can be seen that the propagation through the SI takes the most time. Followed by a high propagation time for the thicker layers as for example fat 2 for the maximum Type 2. The travel time variations between the minimum tickness and maximum thickness is for fat 1 equal to 0.6 ns, for muscle 0.2 ns, for fat 2 0.1 ns and skin 0.01 ns, from which it can be concluded that the influence of thickness variation of skin is not significant for the total travel time. The total travel times for different frequencies and the three human types can be calculated by inserting the results of (15) and (17) into (20) and are listed Table VIII. The total travel time results show a variation of 1 ns for all frequencies when comparing the smallest with the largest tissue thicknesses for the human types.
The cumulative travel time behavior vs. the distance for the different tissue thicknesses of human Type 2 for 403.5 MHz, 916.5 MHz and 2.45 GHz is shown in Figure 4. The total travel time with the minimum layer thickness for 403.5 MHz is 0.94 ns and with the maximum thickness it is equal to 1.35 ns. For 916.5 MHz the total travel time varies from 0.86 to 1.25 ns and for 2.45 GHz between 0.8 ns and 1.2 ns for the minimum and maximum tissue thicknesses. The curves of 916.5 MHz and 2.45 GHz remain for the whole propagation through the layers below the curve of the 403.5 MHz band. This is in accordance to the expectations as the group velocity of the 403.5 MHz band is for all layers smaller than of the other frequencies. From the figure it can be concluded that the travel time of the signal depends not only on the layer thickness but also depends on the group velocity. The slope of the plotted travel time vs. distance indicates the inverse of

TABLE VII: Travel time for different human types at 403.5 MHz

Tissue layers	Travel time in ns					
	Type1		Type2		Type3	
	Min	Max	Min	Max	Min	Max
SI	0.325	0.325	0.325	0.325	0.325	0.325
Fat 1	0.109	0.261	0.268	0.341	0.341	0.711
Muscle	0.200	0.400	0.200	0.400	0.200	0.400
Fat 2	0.123	0.247	0.123	0.247	0.145	0.239
Skin	0.025	0.037	0.025	0.037	0.025	0.037
Total	0.782	1.269	0.942	1.349	1.036	1.711

TABLE VIII: Total travel time for different human types

Frequency	Total travel time in ns					
	Type1		Type2		Type3	
	Min	Max	Min	Max	Min	Max
403.5 MHz	0.782	1.269	0.942	1.349	1.036	1.711
916.5 MHz	0.699	1.166	0.858	1.246	0.952	1.608
2.45 GHz	0.661	1.124	0.820	1.204	0.915	1.566

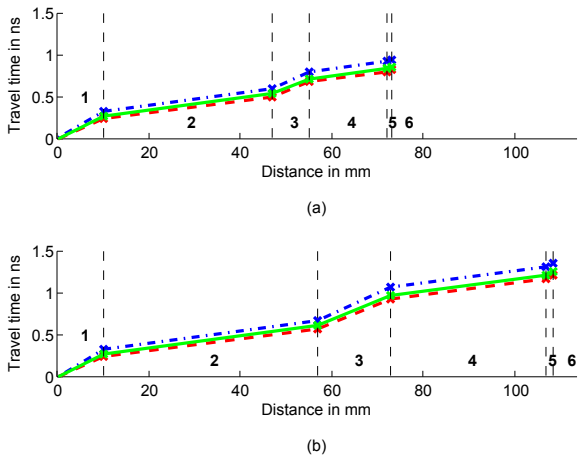

Fig. 4: Travel time vs. distance in a Type 2 human for minimum (a) and maximum (b) tissue layer thicknesses for 403.5 MHz (blue/dash-dot line), 916.5 MHz (green/solid line), and 2.45 GHz (red/dashed line) for different the tissue constellation as in Figure 3

the group velocity in the different layers. The relative travel time of the signal in the SI is comparable to this of fat 1 for all the frequencies. This is due to the lower propagation speed in the SI layer. The propagation speed variations of the SI and the muscle layers have the most influence on the total travel time differences between the frequency bands. The slopes of the other layers are parallel to each other, which means that they are nearly the same for all the frequency bands. The travel time value of the SI tissue is for the lowest frequency one third of the total travel time and one sixth for the highest frequency and the thickest human type. This means that the travel time depends significantly on the depth of the sensor inside the human intestines. The variations in the skin are not visible for all the frequencies.
As a result it can be seen that the travel times do not vary much for the different frequencies. This results can be used to apply TOA measurements for in-body sensor ranging.

C. Absorption

Information about the attenuation of the signal from in-body to on-body is required for RSS based ranging This section analyzes the different sources of signal attenuation for in-body signal propagation. The attenuation of the signal through the body is the sum of losses due to different effects: material losses, reflections, and multiple reflections.

1) Material loss: The human body tissues are lossy materials. Signals are absorbed and therefore attenuated when propagating from the inside to the outside of the body. This absorption due to the characteristics of the propagation medium can be calculated from (6) by using the attenuation constant of the complex propagation formula and the propagation distance. The values of the attenuation constants of the different tissues for the three frequency bands are presented in Table IX. The attenuation constant values for the different tissues and frequencies have a great variance; from an absorption of several nepers per meter to tenths of nepers per meter. A difference in attenuation of 40 neper per meter is calculated for the SI tissue between 403.5 MHz and 2.45 GHz. The higher the frequency the higher the material absorptions will become for all tissue types. The absolute power attenuation of the signal due to the material absorption can be calculated by:

$$L_{\mathrm{A}} = e^{2\alpha z}, \tag{21}$$

where α is the attenuation constant of the RF signal and z is the traveled distance of the signal. The absorption loss in decibels can be calculated by:

$$L_{\mathrm{A_{dB}}} = 20\log_{10} e^{\alpha z} = 8.686\alpha z. \tag{22}$$

This formula can be extended to calculate the attenuation losses of the whole multilayer model. The formula to calculate the total absolute attenuation loss for the combined tissue layers can be described as a summation of the absorption losses (in dB) of each layer:

$$L_{\mathrm{A_{total}}} = \sum_{i=1}^{N} 8.686\alpha_i d_i, \tag{23}$$

where N is the number of tissue layers of the multilayer model, d_i the thickness of the layer, and α_i the attenuation constant of the tissue type. The attenuations are calculated according to the multilayer model and human types, and is presented in Table X for the European MICS frequency band. For the minimum tissue thickness values of Type 1 the total attenuation due to the material absorption is about 6 dB, which is a factor 4 attenuation in power. For the maximum tissue thickness constellation of Type 3 the signal is attenuated by a factor 10. The same calculations are performed for the other frequency bands and an overview of the total material losses for all frequency bands is presented in Table XI. The attenuation factor of the input signal is varying from 4 to 200. Minimum loss occurs for the Type 1 human at 403.5 MHz and maximum loss occurs for the Type 3 human at 2.45 GHz. The receivers need to be able to measure these signal strength variations and thus need to have a large dynamic range. The attenuation of the different tissue layers averaged over the human types is shown in Table XII. For the three most inner tissue layers the average attenuation for 2.45 GHz is 3 dB higher than the average attenuation of those for 403.5 and 916.5 MHz. For the two thinner outer layers, fat 2 and skin, the

TABLE IX: Attenuation constant of different tissue layers and different centre frequencies

Tissue	Attenuation constant α in Np/m]		
	403.5 MHz	916.5 MHz	2.45 GHz
SI	38.44	50.24	79.24
Fat 1	3.23	4.10	8.18
Muscle	19.11	23.81	44.82
Fat 2	3.23	4.10	8.18
Skin	18.15	24.99	44.19

TABLE X: Attenuation due to material absorption for different human types at 403.5 MHz

Tissue layers	Attenuation in dB					
	Type1		Type2		Type3	
	Min	Max	Min	Max	Min	Max
SI	3.34	3.34	3.34	3.34	3.34	3.34
Fat 1	0.42	1.01	1.04	1.32	1.32	2.75
Muscle	1.33	2.66	1.33	2.66	1.33	2.66
Fat 2	0.48	0.95	0.48	0.95	0.56	0.93
Skin	0.17	0.25	0.17	0.25	0.17	0.25
Total	5.74	8.21	6.35	8.52	6.72	9.92

TABLE XI: Total absorption loss for the different frequency bands

Frequency	Absorption loss in dB					
	Type1		Type2		Type3	
	Min	Max	Min	Max	Min	Max
403 MHz	5.74	8.21	6.35	8.52	6.72	9.92
916.5 MHz	7.40	10.51	8.18	10.90	8.64	12.68
2.45 GHz	12.69	18.70	14.26	19.48	15.18	23.03

TABLE XII: Attenuation of all tissues averaged over the human types

Tissue	Average attenuation in dB		
	403.5 MHz	916.5 MHz	2.45 GHz
SI	3.34	4.36	6.88
Fat 1	1.31	1.66	3.32
Muscle	1.99	2.48	4.67
Fat 2	0.72	0.92	1.84
Skin	0.21	0.29	0.52
Total	7.58	9.72	17.22

attenuation variation is only 0.3 dB to 1 dB between the lowest and highest frequency. The total average attenuation between the 403.5 and 916.5 MHz bands differ by only 2 dB. For 2.45 GHz the attenuation is 10 dB higher than the attenuation of the 403.5 MHz. The attenuation seems to increase linearly with frequency by 4.75 dB per GHz. This attenuation per frequency is calculated based on the three average attenuation values for the three different frequency bands.

2) Reflection loss: In addition to the described attenuation due to the lossy material characteristics of the human body, reflection and transmission losses are present when propagating from one layer to the other. Parts of the electric and magnetic fields of the propagating RF wave will be reflected and other will be transmitted. From electromagnetic theory reflected and transmitted intensity for waves at normal incidence to the medium will be determined in this section.
The reflection coefficient can be calculated from the intrinsic impedance of the medium in which the signal is propagating. The intrinsic impedance for a general medium can be calculated as [51]:

$$\eta_i = \frac{j\omega\mu}{\gamma_i}. \tag{24}$$

The reflection coefficient at the boundary of layer i and the next layer $i+1$ follows from [51]:

$$\Gamma_{i,(i+1)} = \frac{\eta_{(i+1)} - \eta_i}{\eta_{(i+1)} + \eta_i} = -\Gamma_{(i+1),i}. \tag{25}$$

The complex reflection coefficient can also be determined by using the index of refraction n_i instead of using the intrinsic impedance η_i of the material. This is described by [50], [53]:

$$n_i = \sqrt{\frac{\varepsilon\mu}{\varepsilon_0\mu_0}} = \sqrt{\varepsilon_{\mathrm{r},i}\mu_{\mathrm{r}}}, \tag{26}$$

where $\varepsilon_{\mathrm{r,i}}$ is the relative permittivity, including the real and imaginary parts of the permittivity. With this formula the reflection coefficients can be calculated for all the layers as well. This reflections coefficients were calculated, and gave the same results for the three frequencies and all the boundaries. From this the reflected power and therefore also the transmitted power can be calculated. The transferred power factor G_T of an incident wave propagating from one layer to another can be calculated as [51], [54]:

$$G_{\mathrm{T}i,(i+1)} = \frac{P_{\mathrm{t}}}{P_{\mathrm{in}}} = 1 - |\Gamma_{i,(i+1)}|^2, \tag{27}$$

where P_{in} is the power of the wave incident to layer i and P_{t} is the transmitted power into the next layer. Figure 5 shows the power definitions of the wave propagation through layers i and $i+1$. The power reflection factor G_{R} and the reflected power P_{R} are already included, because they will be introduced and are required for the calculations of the multiple reflections in next section. The transferred power factor can be expressed in dB and summed up for all layers of the multilayer model by:

$$G_{\mathrm{T}_{\text{total dB}}} = \sum_{i=1}^{N} 10\log_{10}\left(1 - |\Gamma_{i,i+1}|^2\right). \tag{28}$$

With this formula the total loss due to the reflections on each boundary can be calculated. The losses on each boundary between the different tissue layers are shown in Table XIII. Important to note is that the transmission losses of the lower frequencies are higher than those of a higher frequency.
The absorption loss due to the material and the transmission loss due to the reflections together form the absolute power loss of the signal when propagating through multiple layers. These losses are only the losses which occur when the signal is traveling on a direct path through the different layers. In addition to the direct transmission path there are multiple reflection and transmission paths which contain part of the signal power. The multiple reflections and the contribution to the total absorption losses is analyzed in the next paragraph.

3) Multiple reflection loss: Multiple reflections and transmissions between the different layers exist. The reflected wave of one layer can reflect on the boundary of the layer before and again reflect in the direction of the propagation of the direct signal. These multiple reflected and transmitted signals can have a contribution to the total signal. In Figure 6 a signal and its multiple reflections are shown for a general tissue layer.

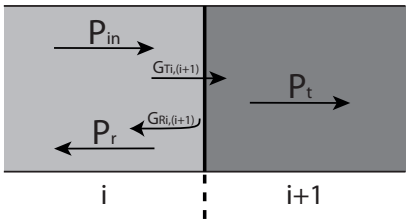

Fig. 5: Power definitions on the boundary between two layers

TABLE XIII: Transferred power factors at each layer boundary and total transferred power factors

Layer boundary	Transferred power factor in dB		
	403.5 MHz	916.5 MHz	2.45 GHz
$G_{\mathrm{T}1,2}$	-2.25	-1.76	-1.51
$G_{\mathrm{T}2,3}$	-1.54	-1.42	-1.39
$G_{\mathrm{T}3,4}$	-1.54	-1.42	-1.39
$G_{\mathrm{T}4,5}$	-1.34	-1.15	-1.05
$G_{\mathrm{T}5,6}$	-3.96	-3.51	-3.28
$G_{\mathrm{T}total}$	-10.63	-9.26	-8.62

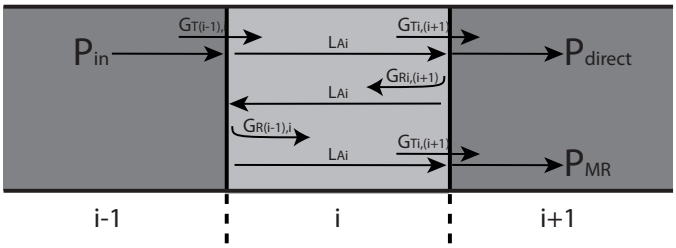

Fig. 6: Multiple reflection path

The reflected power factor must be calculated first. The reflected power factor can be determined in the same way as the transferred power factor. Therefore, the formula to calculate the reflected power factor G_R for the power which is reflected back from the boundary is equal to:

$$G_{\mathrm{R}i,(i+1)} = \frac{P_{\mathrm{r}}}{P_{\mathrm{in}}} = |\Gamma_{i,(i+1)}|^2. \tag{29}$$

The attenuation in dB for the reflection on different boundaries and for different frequencies is shown in Table XIV. The negative power gain of the absolute reflected power on the different boundaries are in contrast to the transmission power gains lower for higher frequency than for lower frequencies. This results in a higher attenuation of the signal when reflecting on an interface. The difference in loss is only 0.5 dB for the different frequencies at the boundaries of layers (2,3), (3,4), and (5,6). For the boundary between layer 1 and layer 2 the difference in loss between the frequencies is about 1.5 dB and for the boundary between fat 2 and skin the difference in loss is 1 dB. On average 1.5 dB (70%) of the incident signal on a boundary is transferred to the next layer and 5 dB (30%) is reflected back into the layer.

As shown in Figure 6 the input signal is first attenuated due to the transmission loss on the boundary between the layers $i-1$ and i, and obtains attenuation due to the material loss ($L_{\mathrm{A}i}$). Afterwards it experiences transmission losses from the boundary between the layers i and $i+1$ before continuing in layer $i+1$. Part of the signal is reflected back at the last boundary and will propagate in the reverse direction to the boundary between the layers i and $i-1$. There the signal will be reflected again and will propagate to the boundary between the layers i and $i+1$ where part of the signal will be transmitted into layer $i+1$. The difference in power attenuation of this multiple reflection G_{MR} and the direct path P_{direct} is thus: two times the material absorption, one reflection gain at boundary $(i-1,i)$, and one reflection gain boundary $(i,i+1)$. Therefore, the power difference between the direct power attenuation and the multiple reflection attenuation is dependent on the following three variables:

$$G_{\mathrm{MR}} = G_{\mathrm{Ri,(i+1)}} - 2\ L_{\mathrm{A}i} + G_{\mathrm{R}(i-1),i}. \tag{30}$$

The variables are used as defined previously (see Figure 6). To demonstrate the use of these formulas an example calculation is done for the layer fat 1 between the small intestine and the muscle layer. For a Type 2 human body with the maximum tissue thickness values the signal losses are therefore:

$$\begin{aligned} G_{MR} &= -5.24 - 2 \cdot 1.32 - 3.93 \\ &= -11.81 \text{ dB} \end{aligned}$$

The difference of the multiple reflection signal and the signal in the direct path is equal to about 11.8 dB. This means that the multiple reflected signal is much smaller than the direct transmitted signal thus does not contribute significantly to the total signal.

The reflected power factors of all tissues are about the same size. As a result, the attenuation of the multiple reflected signals will always be significantly smaller than the direct path through a layer.

4) Total absorption loss: The total loss in human Type 2 is shown for different frequencies in Figure 7. The total loss for 403.5 MHz with the minimum layer thickness is 17 dB and with the maximum thickness it is equal to 19.2 dB. The total loss varies from 17.4 dB to 20.2 dB for the minimum and maximum tissue thicknesses for 916.5 MHz and between 22.8 dB and 28.0 dB for 2.45 GHz. When looking at the fat tissue layers of all the figures it can be seen that the material absorption in these layers is low. There is only a small fall of in signal power for all frequencies for the fat layers. For thicker layers the attenuation stays small as it was expected from the attenuation constants. The attenuation due to transferring into the next layers on the boundaries to the fat layers is almost

TABLE XIV: Reflected power factors at each layer boundary

Layer Boundary	Reflected power factor in dB		
	403.5 MHz	916.5 MHz	2.45 GHz
$G_{\mathrm{R1,2}}$	−3.93	−4.77	−5.32
$G_{\mathrm{R2,3}}$	−5.24	−5.53	−5.63
$G_{\mathrm{R3,4}}$	−5.24	−5.53	−5.63
$G_{\mathrm{R4,5}}$	−5.77	−6.35	−6.67
$G_{\mathrm{R5,6}}$	−2.23	−2.56	−2.76

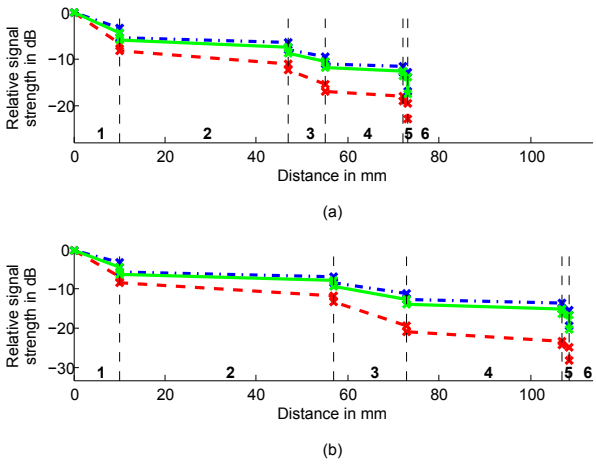

Fig. 7: Total power transfer in a Type 2 human for minimum (a) and maximum (b) tissue layer thicknesses for 403.5 MHz (blue/dash-dot line), 916.5 MHz (green/solid line), and 2.45 GHz (red/dashed line) for different the tissue constellation as in Figure 3

constant for all frequencies. The transferred power loss which occurs on boundary (5,6) is much higher than on the other boundaries. This is due to the high reflections which occur because of the intrinsic impedance change from 48 – 60 Ω for the skin tissue, depending on the operation frequency, to 377 Ω of air. The graphs indicate that the losses in the SI and muscle layer are the biggest which can be seen from the slope of the graphs. The total power transfer between the minimum and thicknesses for the frequencies differ about 2 dB, 3 dB, and 5 dB which is a small number in decibel, in power reduction the maximum tissue types are 1.6, 2, and 4 times bigger than the minimum tissue thickness power transfer. These differences are mainly caused by the difference in muscle tissue thickness, since muscle tissue has together with the SI tissue the highest attenuation constant and the thickness of the SI was fixed for this calculations. Actually the sensor location can be much deeper inside the SI tissue layer which would result in a higher total power reduction.
The differences in power loss are only several dB which is a small amount for telecommunication systems. The results of this analysis gives more insight in the causes of attenuation and can be used to make ranging of a in-body located sensor with RSS measurements possible.

V. Conclusion

In this research the radio propagation inside a human body has been analyzed by investigating the physical characteristics of a new developed multilayer model.
A novel method of calculating the absolute losses and travel times of the propagation path has been introduced. The performed numerical analysis is independent of the measurement environment, equipment or antenna mismatches. The propagation path is determined not by averaging tissue characteristics but rather including the influences of all tissue layers from in-body to on-body, based on a new multilayer model. The benefits of the developed multilayer model are that it is easy to adjust and to extend. This analysis takes the complex tissue characteristics into account both for the travel time as for signal strength analysis. New insights on the different types of absorptions are gathered. The propagation loss and travel time analysis is done for different human types and different frequencies.

The losses due to the impedance differences between the layers are of significant value and almost the same for all frequencies. The signal attenuation inside fat layers is small such that there are no big differences in the attenuation for different thicknesses of fat layers. The attenuation due to muscle tissue layer variation and SI tissue layer thickness cause big attenuation differences for all frequency bands.
For the determination of the travel times the group velocity as propagation speed is considered rather than the phase velocity. Furthermore, the conductivity characteristics of human tissue are included in these calculations. The resulting group velocity in the lossy human body tissue material differs significantly from the phase velocity calculations of lossless material as it was assumed in literature. The SI and muscle tissue layers give the most influence on the travel time for all frequency bands. The propagation delay due to the fat layers are the same for the different frequencies.
From the results it is investigated that the absorption and delay are not that frequency dependent as is expected and mentioned in literature. This can be due to the limited number of effects which are analyzed or the other characteristics which have been taken into account. An important conclusion is that reflections on the boundaries have major impact on the attenuation.

In future work the influence of oblique incidence on the power attenuations and reflections have to be investigated as well as other effects as multipath and diffraction. The physical multilayer model should also be extended to a 2D/3D model to gain more insight into the absorptions and travel times changes. Attenuation due to reflections have to be considered for a deeper location of the endoscopy capsule in the small intestines. After that the possibility of implementing localization could better be assessed. A statistical model has to be developed to take different human types and effects into account for the real localization of a sensor inside the human body.

From the research it can be concluded that describing and analyzing in-body radio propagation is challenging for localization purposes.

References

[1] UNFPA and H. International, "Ageing in the twenty-first century: A celebration and a challenge," p. 190, 2012, iSBN: 978-0-89714-981-5.

[2] G. Iddan, G. Meron, A. Glukhovsky, and P. Swain, "Wireless capsule endoscopy," *Nature*, vol. 405, p. 417, 2000.

[3] M. E. Riccioni, R. Urgesi, R. Cianci, A. Bizzotto, C. Spada, and G. Costamagna, "Colon capsule endoscopy: Advantages, limitations and expectations. which novelties?" *World journal of gastrointestinal endoscopy*, vol. 4, no. 4, p. 99, 2012.

[4] W. A. Qureshi, "Current and future applications of the capsule camera," *Nature reviews drug discovery*, vol. 3, no. 5, pp. 447–450, 2004.

[5] H. Cao, V. Leung, C. Chow, and H. Chan, "Enabling technologies for wireless body area networks: A survey and outlook," *IEEE Communications Magazine*, vol. 47, no. 12, pp. 84–93, 2009.

[6] M. Chen, S. Gonzalez, A. Vasilakos, H. Cao, and V. C. Leung, "Body area networks: A survey," *Mobile Networks and Applications*, vol. 16, no. 2, pp. 171–193, 2011.

[7] K. Arshak and F. Adepoju, "Capsule tracking in the GI tract: a novel microcontroller based solution," in *Proceedings of the IEEE Sensors Applications Symposium, 2006.* IEEE, 2006, pp. 186–191.

[8] L. Wang, C. Hu, L. Tian, M. Li, and M.-H. Meng, "A novel radio propagation radiation model for location of the capsule in GI tract," in *IEEE International Conference on Robotics and Biomimetics (ROBIO), 2009.* IEEE, 2009, pp. 2332–2337.

[9] P. Arab, M. Heimlich, and E. Dutkiewicz, "Investigation of radar localization system accuracy for human gastro intestine (GI) tract," in *7th International Symposium on Medical Information and Communication Technology (ISMICT), 2013.* IEEE, 2013, pp. 144–148.

[10] U.S. National Library of Medicine, "The visible human project - color cryosections," January 1993. [Online]. Available: http://www.nlm.nih.gov/research/visible/photos.htm

[11] A. Taparugssanagorn, A. Rabbachin, M. Hämäläinen, J. Saloranta, J. Iinatti *et al.*, "A review of channel modelling for wireless body area network in wireless medical communications," University of Oulu. Citeseer, 2008.

[12] K. Pahlavan, Y. Ye, R. Fu, and U. Khan, "Challenges in channel measurement and modeling for RF localization inside the human body," *International Journal of Embedded and Real-Time Communication Systems (IJERTCS)*, vol. 3, no. 3, pp. 18–37, 2012.

[13] C. Gabriel, "Compilation of the dielectric properties of body tissues at RF and microwave frequencies." Defense Technical Information Center, Tech. Rep., 1996.

[14] D. Andreuccetti, R. Fossi, and C. Petrucci, "An internet resource for the calculation of the dielectric properties of body tissues in the frequency range 10 Hz - 100 GHz," 1997, based on data published by C. Gabriel et al. in 1996. [Online]. Available: http://niremf.ifac.cnr.it/tissprop/

[15] S. Gabriel, R. Lau, and C. Gabriel, "The dielectric properties of biological tissues: II. measurements in the frequency range 10 Hz to 20 GHz," *Physics in medicine and biology*, vol. 41, no. 11, p. 2251, 1996.

[16] H. S. Savci, A. Sula, Z. Wang, N. S. Dogan, and E. Arvas, "MICS transceivers: regulatory standards and applications [medical implant communications service]," in *Proceedings. IEEE SoutheastCon, 2005.* IEEE, 2005, pp. 179–182.

[17] "IEEE standard for local and metropolitan area networks - part 15.6: Wireless body area networks," *IEEE Std 802.15.6-2012*, pp. 1–271, Feb 2012.

[18] R. Chavez-Santiago, K. Sayrafian-Pour, A. Khaleghi, K. Takizawa, J. Wang, I. Balasingham, and H.-B. Li, "Propagation models for IEEE 802.15. 6 standardization of implant communication in body area networks," *IEEE Communications Magazine*, vol. 51, no. 8, 2013.

[19] M. Hamalainen, A. Taparugssanagorn, R. Tesi, and J. Iinatti, "Wireless medical communications using UWB," in *IEEE International Conference on Ultra-Wideband, 2009.* IEEE, 2009, pp. 485–489.

[20] J. Chen, "UWB characteristics of RF propagation for body mounted and implanted sensors," Ph.D. dissertation, Worcester Polytechnic Institute, 2013.

[21] K. Y. Yazdandoost, "UWB antenna for body implanted applications," in *9th European Radar Conference (EuRAD), 2012.* IEEE, 2012, pp. 606–609.

[22] K. Y. Yazdandoost, "A 2.4 GHz antenna for medical implanted communications," in *Asia Pacific Microwave Conference, 2009.* IEEE, 2009, pp. 1775–1778.

[23] M. Kesler, "Highly resonant wireless power transfer: Safe, efficient, and over distance," WiTricity Corporation, 2013.

[24] M. Coimbra and J. Cunha, "MPEG-7 visual descriptors - contributions for automated feature extraction in capsule endoscopy," *IEEE Transactions on Circuits and Systems for Video Technology*, vol. 16, no. 5, pp. 628–637, May 2006.

[25] M. Coimbra, P. Campos, and J. S. Cunha, "Topographic segmentation and transit time estimation for endoscopic capsule exams," in *IEEE International Conference on Acoustics, Speech and Signal Processing, 2006.*, vol. 2. IEEE, 2006, pp. II–II.

[26] J. Bulat, K. Duda, M. Duplaga, R. Fraczek, A. Skalski, M. Socha, P. Turcza, and T. Zielinski, "Data processing tasks in wireless GI endoscopy: image-based capsule localization & navigation and video compression," in *29th Annual International Conference of the IEEE Engineering in Medicine and Biology Society, 2007.* IEEE, 2007, pp. 2815–2818.

[27] U. I. Khan, "Computational techniques for comparative performance evaluation of RF localization inside the human body," Ph.D. dissertation, Worcester Polytechnic Institute, 2011.

[28] S. Gezici, Z. Tian, G. B. Giannakis, H. Kobayashi, A. F. Molisch, H. V. Poor, and Z. Sahinoglu, "Localization via ultra-wideband radios: a look at positioning aspects for future sensor networks," *IEEE Signal Processing Magazine*, vol. 22, no. 4, pp. 70–84, 2005.

[29] A. Alomainy, Y. Hao, Y. Yuan, and Y. Liu, "Modelling and characterisation of radio propagation from wireless implants at different frequencies," in *The 9th European Conference on Wireless Technology, 2006.* IEEE, 2006, pp. 119–122.

[30] W. G. Scanlon, B. Burns, and N. E. Evans, "Radiowave propagation from a tissue-implanted source at 418 MHz and 916.5 MHz," *IEEE Transactions on Biomedical Engineering*, vol. 47, no. 4, pp. 527–534, 2000.

[31] W. G. Scanlon, N. E. Evans, and Z. M. McCreesh, "RF performance of a 418-MHz radio telemeter packaged for human vaginal placement," *IEEE Transactions on Biomedical Engineering*, vol. 44, no. 5, pp. 427–430, 1997.

[32] K. Tai, H. Harada, and R. Kohno, "Channel modeling and signaling of medical implanted communication systems and a step to medical ICT," in *Mobile and Wireless Communications Summit, 2007. 16th IST.* IEEE, 2007, pp. 1–5.

[33] L. C. Chirwa, P. A. Hammond, S. Roy, and D. R. Cumming, "Electromagnetic radiation from ingested sources in the human intestine between 150 MHz and 1.2 GHz," *IEEE Transactions on Biomedical Engineering*, vol. 50, no. 4, pp. 484–492, 2003.

[34] K. Takizawa, H. Hagiwara, and K. Hamaguchi, "Path-loss estimation of wireless channels in capsule endoscopy from X-ray CT images," in *Annual International Conference of the IEEE Engineering in Medicine and Biology Society, EMBC, 2011.* IEEE, 2011, pp. 2242–2245.

[35] J. Ryckaert, P. De Doncker, R. Meys, A. de Le Hoye, and S. Donnay, "Channel model for wireless communication around human body," *Electronics letters*, vol. 40, no. 9, pp. 543–544, 2004.

[36] A. Fort, C. Desset, J. Ryckaert, P. De Doncker, L. Van Biesen, and S. Donnay, "Ultra wide-band body area channel model," in *IEEE International Conference on Communications, 2005.*, vol. 4. IEEE, 2005, pp. 2840–2844.

[37] T. Zasowski, F. Althaus, M. Stager, A. Wittneben, and G. Troster, "UWB for noninvasive wireless body area networks: channel measurements and results," in *IEEE Conference on Ultra Wideband Systems and Technologies, 2003.* IEEE, 2003, pp. 285–289.

[38] T. Zasowski, G. Meyer, F. Althaus, and A. Wittneben, "Propagation effects in UWB body area networks," in *IEEE International Conference on Ultra-Wideband, 2005.* IEEE, 2005, pp. 16–21.

[39] A. Fort, C. Desset, J. Ryckaert, P. De Doncker, L. Van Biesen, and P. Wambacq, "Characterization of the ultra wideband body area propagation channel," in *IEEE International Conference on Ultra-Wideband, 2005.* IEEE, 2005, pp. 6–pp.

[40] M. Kawasaki and R. Kohno, "A toa based positioning technique of medical implanted devices," in *Third International Symposium on Medical Information & Communication Technology, ISMCIT09, Montreal*, 2009.

[41] M. Pourhomayoun, M. Fowler, and Z. Jin, "A novel method for medical implant in-body localization," in *Annual International Conference of the IEEE Engineering in Medicine and Biology Society (EMBC), 2012.* IEEE, 2012, pp. 5757–5760.

[42] M. Pourhomayoun, Z. Jin, and M. Fowler, "Accurate localization of in-body medical implants based on spatial sparsity," *IEEE Transactions on Biomedical Engineering*, vol. 61, no. 2, pp. 590–597, Feb 2014.

[43] A. Camlica, "Least-squares based adaptive source localization with biomedical applications," Master's thesis, University of Waterloo, 2013.

[44] K. Sayrafian-Pour, W.-B. Yang, J. Hagedorn, J. Terrill, and K. Y. Yazdandoost, "A statistical path loss model for medical implant communication channels," in *IEEE 20th International Symposium on Personal, Indoor and Mobile Radio Communications, 2009.* IEEE, 2009, pp. 2995–2999.

[45] K. Pahlavan, G. Bao, Y. Ye, S. Makarov, U. Khan, P. Swar, D. Cave, A. Karellas, P. Krishnamurthy, and K. Sayrafian, "RF localization for wireless video capsule endoscopy," *International Journal of Wireless Information Networks*, vol. 19, no. 4, pp. 326–340, 2012.

[46] P. Brida and J. Machaj, "A novel enhanced positioning trilateration algorithm implemented for medical implant in-body localization," *International Journal of Antennas and Propagation*, vol. 2013, 2013.

[47] P. Swar, K. Pahlavan, and U. Khan, "Accuracy of localization system inside human body using a fast fdtd simulation technique," in *6th International Symposium on Medical Information and Communication Technology (ISMICT), 2012.* IEEE, 2012, pp. 1–6.

[48] U. I. Khan, K. Pahlavan, and S. Makarov, "Comparison of toa and rss based techniques for RF localization inside human tissue," in *Annual International Conference of the IEEE Engineering in Medicine and Biology Society, EMBC, 2011.* IEEE, 2011, pp. 5602–5607.

[49] Y. Kilic, H. Wymeersch, A. Meijerink, M. Bentum, and W. Scanlon, "Device-free person detection and ranging in UWB networks," *IEEE Journal of Selected Topics in Signal Processing*, vol. 8, no. 1, pp. 43–54, Feb 2014.

[50] D. Griffiths, *Introduction to Electrodynamics*, ser. Pearson international edition. Prentice Hall International, 1999.

[51] D. Pozar, *Microwave Engineering*. Wiley, 2012.

[52] C. Furse, D. Christensen, and C. Durney, *Basic Introduction to Bioelectromagnetics, Second Edition*, ser. Biomedical engineering. Taylor & Francis, 2009.

[53] A. Molisch, *Wireless Communications*, ser. Wiley - IEEE. Wiley, 2012.

[54] W. Hayt and J. Buck, *Engineering Electromagnetics*. McGraw-Hill Education, 2011.